Institute of Paper Science and Technology
Atlanta, Georgia

IPST TECHNICAL PAPER SERIES

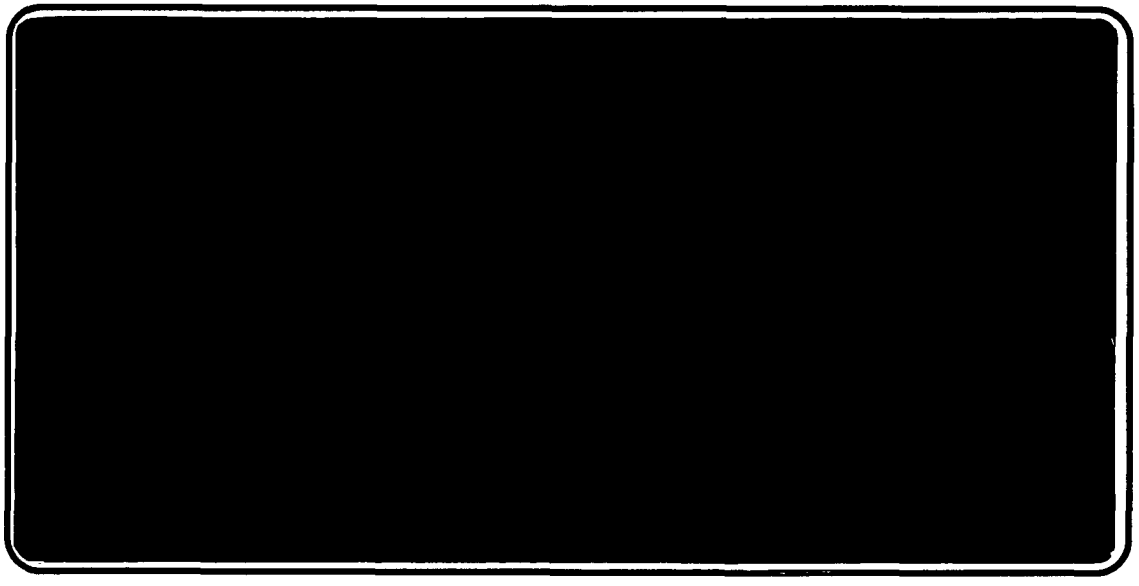

NUMBER 374

DETERMINATION OF GAS TEMPERATURES AT 295-1273 K USING CO VIBRATIONAL-ROTATIONAL ABSORPTION SPECTRA RECORDED WITH A FT-IR SPECTROMETER

P.J. MEDVECZ, K.M. NICHOLS, D.T. CLAY, AND R. ATALLA

MARCH, 1991

Determination of Gas Temperatures at 295-1273 K Using CO Vibrational-Rotational Absorption Spectra Recorded with a FT-IR Spectrometer

P.J. Medvecz, K.M. Nichols, D.T. Clay, and R. Atalla

Submitted for
Applied Spectroscopy

Copyright© 1990 by The Institute of Paper Science and Technology

For Members Only

NOTICE & DISCLAIMER

The Institute of Paper Science and Technology (IPST) has provided a high standard of professional service and has put forth its best efforts within the time and funds available for this project. The information and conclusions are advisory and are intended only for internal use by any company who may receive this report. Each company must decide for itself the best approach to solving any problems it may have and how, or whether, this reported information should be considered in its approach.

IPST does not recommend particular products, procedures, materials, or service. These are included only in the interest of completeness within a laboratory context and budgetary constraint. Actual products, procedures, materials, and services used may differ and are peculiar to the operations of each company.

In no event shall IPST or its employees and agents have any obligation or liability for damages including, but not limited to, consequential damages arising out of or in connection with any company's use of or inability to use the reported information. IPST provides no warranty or guaranty of results.

DETERMINATION OF GAS TEMPERATURES AT 295-1273 K USING CO VIBRATIONAL-ROTATIONAL ABSORPTION SPECTRA RECORDED WITH A FT-IR SPECTROMETER

Patrick J. Medvecz, Kenneth M. Nichols*
The Institute of Paper Science and Technology, 575 14th St., N.W., Atlanta, Georgia, 30318

David T. Clay
James River Corporation, Neenah, WI

Rajai Atalla
Forest Products Laboratory, Madison, WI

ABSTRACT

Fourier transform infrared absorption spectroscopy has been used to determine the rotational temperatures of high temperature (≤ 1273 K) CO/N_2 gas samples. To achieve this objective, a special gas cell was constructed which permitted the acquisition of absorption spectra of samples containing CO at concentrations of 1-10% by volume in N_2 and at temperatures between 295-1273 K. The absorption spectra were recorded using a moderate resolution (0.25 cm^{-1}) FT-IR spectrometer. The rotational temperatures were calculated from the spectra after rigorous correction for photometric errors. Temperatures calculated from the P branch of CO spectra had accuracies of 3.2% or better. In all cases, the calculated temperatures were lower than temperatures recorded with a thermocouple, which had an accuracy of ± 0.75%. An important factor in the success of these determinations was the adoption of measures to prevent the modulated spectral emission of the hot gases from reaching the detector.

INDEX HEADINGS: Infrared, FT-IR, CO, Absorption Spectra, Temperature Analysis, Combustion Gases.

INTRODUCTION

At the Institute of Paper Science and Technology, efforts have been directed toward using Fourier transform infrared (FT-IR) absorption spectroscopy for the *in situ* determination of concentrations and temperatures of the gaseous components formed during laboratory-scale combustion of black liquor. Black liquor forms during the pulping of wood; it is burned to generate high pressure steam and to recycle the inorganic chemicals for reuse as pulping chemicals. Of immediate interest is the development of techniques which would enable quantification of CO and CO_2 and determination of gas phase temperatures near the burning char surface. This information is critical to the development of mathematical models describing the combustion process. The char burning environment is characterized by high temperatures (950-1300 K), intense emission of radiation from molten sodium salts, and the presence of fume (small particles of sodium salts of diameter 0.1-1.0μm). The concentrations of CO and CO_2 vary between 1 and 15%.

Fourier transform infrared absorption spectroscopy has been used previously for *in situ* determination of gaseous species concentrations and temperatures in several different high temperature environments. Ottesen and Stephenson[1] applied the technique for the determination of temperatures and gas concentrations above hydrocarbon flames in the temperature range of 473-1873 K. Ottesen and Thorne performed similar experiments in a coal combustion environment and calculated gas temperatures

*Author to whom correspondence should be sent.

between 1200-1500 K, CO_2 concentrations of approximately 1000-4500 ppm, and CO concentrations of approximately 150-650 ppm.[2,3] Solomon *et al.* used the technique for the identification of the gaseous components formed during coal thermal decomposition (pyrolysis) at temperatures near 1200 K.[4] All of this work has demonstrated the usefulness of FT-IR spectroscopy in acquiring moderate resolution vibrational-rotational absorption spectra in a high temperature, luminous, combustion environment. However, the calculation methodology used by these authors did not correct for some of the factors that can adversely affect FT-IR absorption spectra.

Quantifications of gas concentrations and temperatures in a combustion environment are complicated by several factors: spectral distortions resulting from the finite resolution of the FT-IR instrument, incomplete knowledge of half-widths of the absorption lines at high temperatures (973-1273 K), and the effects of radiative emissions from the hot gas sample. Each of these factors can introduce significant errors in the calculated gas temperatures or concentrations. Thorough consideration of the errors resulting from one of these effects, the finite resolution limitation, has been made by Cleland and Hess[5] and by Anderson and Griffiths[6]. Cleland and Hess performed *in situ* FT-IR absorption spectroscopy measurements in nitrous oxide glow discharges to determine rotational temperatures and the extent of nitrous oxide dissociation. Anderson and Griffiths were successful in using FT-IR for the determination of gas temperatures from CO absorption spectra recorded from pure CO or CO/air samples. Both of these works, however, included temperature calculations from spectra at temperatures only as high as 425 K. This temperature is well below the 1300 K combustion environment of black liquor char. To our knowledge there have been no studies measuring temperatures and concentrations that use FT-IR absorption spectroscopy at temperatures between 425 K and 1300 K and take into account the effects noted above.

In addition to the difficulties described above, absorption spectra recorded in combustion environments can be further complicated by nonuniformities along the infrared beam path. Calculations for both concentrations and temperatures are based upon the assumption that the gas sample is uniform with respect to temperature and composition. Therefore, before spectra recorded in the black liquor combustion environment are evaluated, it is necessary to establish the procedures by making both temperature and concentration measurements from absorption spectra in a more simple and controlled environment. This study focuses on efforts to determine rotational temperatures in such an environment. The intent of this work is to extend the work of Anderson and Griffiths and Cleland and Hess into the temperature range of interest for black liquor combustion.

THEORY

A brief description of the calculation of gas temperatures from absorption spectra of diatomic molecules is given here. Greater detail is provided by Gross *et al.*[7] and by Anderson and Griffiths[6].
The relationship between the absorption intensity of a diatomic molecule and the energy of the transition is given by

$$S(m) \propto |m| \cdot F(m) \cdot \nu(m) \cdot \exp(-E(m)/(k \cdot T)) \qquad (1)$$

where m is the index of the absorption line, S(m) is the intensity of the absorption line, F(m) is the Herman-Wallis correction factor[6], $\nu(m)$ is the frequency of the absorption line, E(m) is the energy of the transition, k is the Boltzmann constant, and T is the gas temperature. For the R branch, the value of m is equal to J"+1, and for the P branch, the value of m equals -J", where J" is the rotational quantum number of the lower state. This equation can be rearranged into the form

$$\ln(S(m)/(|m| \cdot F(m)\nu(m))) \propto -E(m)/(k \cdot T). \qquad (2)$$

A plot of $\ln(S(m)/(|m|\cdot F(m)\cdot v(m)))$ vs. $E(m)/k$ should yield a straight line with a slope equal to $-1/T$. With the exception of the line intensity, all the variables in Equation 2 are readily obtained. Therefore, when the intensity of several vibrational-rotational absorption lines from either the P or the R branch are known, Equation 2 can be used to obtain the gas temperature.

For gases at atmospheric pressure, collisional broadening is the dominant line broadening mechanism, and therefore, a Lorentzian line shape is assumed for the absorption of infrared radiation by the molecule.[7] The line intensity is then given by[6]

$$S(m) = \pi\cdot(\ln 10)\cdot A_{peak}\cdot\gamma \qquad (3)$$

where A_{peak} is the absorbance at the peak maximum and γ is the half-width at half-height. The use of this equation is complicated by two factors: first, the absorbance peaks are distorted by the finite resolution of the instrument, which contributes to what is known as the photometric error, and second, half-widths must be known at high temperatures.

Photometric Error

The distortion of spectral peaks resulting from the finite resolution of the instrument occurs because the intensity measured by the instrument at any given frequency is actually an average intensity of all the frequencies within the spectral bandpass of the instrument. The extent of this error is dependent upon the resolution of the instrument and the half-width of the absorption line. Anderson and Griffiths[8] have given a thorough theoretical analysis of this phenomenon.

The mathematical relationship between experimentally obtained (or apparent) peak heights (A^a_{peak}) and true peak heights (A^t_{peak}) is given in Equation 4,

$$A^a_{peak} = -\log\left[\int_0^\infty 2\cdot(\sin^2(\pi\cdot y)/(\pi\cdot y)^2)\cdot\exp(-\ln 10\, A^t_{peak}/(1+4\rho^2y^2))\, dy\right]. \qquad (4)$$

The variables y and ρ are defined as,

$$y = (\nu - \nu_o)/R \qquad (5)$$

$$\rho = R/(2\gamma) \qquad (6)$$

where $(\nu - \nu_o)$ is the frequency difference between υ and the peak maximum at ν_o, R is the resolution of the spectrometer and γ is the half-width of the line at half height. The experimental peak heights are the peak values recorded by the FT-IR instrument; the true peak heights are the peak heights due only to absorption of infrared radiation by the gas. Equation 4 describes the experimentally measured peak heights as the convolution of two functional parts. The first part, $(\sin^2(\pi\cdot y)/(\pi\cdot y)^2)$, is known as the line shape (LS). The LS describes the response of the instrument to radiation of frequency υ when the instrument is measuring at frequency ν_i. The functionality of the LS changes according to the type of apodization, which is applied to the interferogram before transformation. Apodization is the process of multiplying the interferogram by a mathematical function to change the shape of the peaks in the transformed spectrum. It is most commonly done to reduce the negative side lobes which would otherwise appear next to absorption peaks if no apodization function was used. The description of the LS in Equation 4 is a result of triangular apodization.[9] The second part, $\exp(-\ln 10\, A^t_{peak}/(1+4\rho^2y^2)$, describes the absorption of infrared radiation by the sample assuming a Lorentzian line shape.

Equation 4 provides the means to correct absorption peaks for the photometric error. Difficulties arise in its use, however, since γ is a temperature dependent quantity. This implies that the temperature must be known before the peak heights can be corrected. Anderson and Griffiths[6] circumvented this problem by using an iterative nonlinear least squares computation procedure, with temperature as one of the adjustable parameters in order to solve for the gas temperature. In this work, a similar iterative procedure has been developed; it accounts for both the change of peak widths with temperature and the photometric error distortions. This method will be described in greater detail below.

High Temperature Half-Width Data

The extent of photometric error correction is determined by the ratio of $R/(2\gamma)$, and therefore, the half-width of an absorption line is a key parameter in the determination of true peak heights. For gases at atmospheric pressure, collision broadening controls the line shape.[7] With this mechanism of line broadening, each species in the gas sample influences the width of the line being observed. In addition, the half-width is influenced by the value of m and the gas temperature. Equations have been developed to describe the half-width of absorption lines, $\gamma_X(m)$, in gas mixtures based upon the partial pressure of the gaseous components, P_X, P_Y, *etc.*; the total pressure, P_T; broadening coefficients, $\gamma^o_{X,X}(m)$, $\gamma^o_{X,Y}(m)$, *etc.*; the gas temperature, T; a reference temperature, T^o; and the temperature exponents, $N_{X,X}(m)$, $N_{X,Y}(m)$, *etc.*[7] For example, broadening for a two-component system consisting of species x and y is given by,

$$\gamma_X(m) = \gamma^o_{X,X}(m)\cdot(P_X/P_T)\cdot(T^o/T)^{N_{X,X}(m)} + \gamma^o_{X,Y}(m)\cdot(P_Y/P_T)\cdot(T^o/T)^{N_{X,Y}(m)}. \quad (7)$$

Details describing this equation and the theories used to derive it are presented in greater detail by Gross *et al.*[7] Equation 7 yields the line half-widths required in Equation 6 for photometric error corrections and subsequent temperature calculations. In order to use Equation 7, however, either experimental or theoretical temperature and m dependent values of $\gamma^o_{X,X}(m)$, $\gamma^o_{X,Y}(m)$, $N_{X,X}(m)$, and $N_{X,Y}(m)$ are required. To the best of our knowledge, neither experimental values nor theoretical predictions exist which can completely account for all the lines used in this work within the temperature range of 300-1300 K.

Recently, Hartmann *et al.*[10] developed a model which accounts for CO line broadening by H_2O, N_2, O_2, and CO_2. This model is based, in part, on existing high temperature experimental broadening data and upon theoretical considerations. Their calculations have yielded values of γ^o and N, including their dependence on m, which can be used in Equation 7 to calculate CO half-widths. This appears to be the most comprehensive database available from which high temperature CO half-width information can be obtained. Where applicable, these values have been used for photometric error correction and temperature calculations in this work. However, these data have two limitations: first, there are minimum temperature requirements for the use of the broadening coefficients and temperature exponents, and second, the model does not yield predictions for CO self-broadening. Where this model cannot be used, reliable values for room temperature nitrogen broadening coefficients of CO reported by Varghese and Hanson[11] and Nakazawa and Tanaka[12] are used. Similarly, values of CO self-broadening coefficients have been reported by Nakazawa and Tanaka[12] and by Anderson and Griffiths[6]. When these data must be used, the temperature exponent is assumed to be a constant, independent of both the broadening species and m value. The value of 0.75 is used for the temperature exponent, as described by Gross *et al.*[7] The reliability of the model presented by Hartmann *et al.*[10] for high temperature, CO line broadening calculations will be discussed later.

Emission

In addition to complications resulting from photometric errors and half-width determinations, emission radiation from a high temperature gas sample can also complicate an absorption spectrum. The absorption peaks used for temperature determination in this work are a result of the transitions from the ground state to the first excited state in the P branch. Emission from the opposite transition, from the first excited state to the ground state, is of the same frequency. If this emission becomes modulated and then reaches the detector, the intensity of the absorption peaks will be reduced. The intensity of an emission line has a fourth order dependence on frequency as follows,

$$S(m) \propto |m| \cdot F(m) \cdot \nu(m)^4 \cdot \exp(-E(m)/k \cdot T) \qquad (8)$$

as compared to the first order dependence for absorption lines[7]. Because of the difference in the power of the frequency term in these two equations (1 and 8), adding emission lines to the absorption lines will destroy the temperature relationship described by Equation 2. It is essential to accurate temperature calculations that this radiation source be eliminated. In order to eliminate the effect of emission, it is best to simply prevent the emission from the cell from becoming modulated and reaching the detector. This can be accomplished by the use of an aperture between the interferometer and the gas cell. The placement of this aperture is discussed later.

TEMPERATURE CALCULATION METHODOLOGY

Calculations of gas temperatures from CO absorption spectra have been made by incorporating the theoretical concepts presented by Anderson and Griffiths[6,8] into a computational program written in Pascal. The program includes corrections for photometric errors and takes advantage of the best available high temperature CO line broadening data. Reduction or elimination of errors due to emission was based on modification of the experimental optical configuration.

After a CO absorption spectrum was recorded, the heights and positions of the absorption lines were determined using software written by Laser Precision Analytical. This program conveniently writes the data to an ASCII file. The ASCII file is then read by the temperature calculating program, which finds the peaks corresponding to CO absorption. Of those lines corresponding to absorption by CO, any combination of lines could be selected for use in temperature calculations. For this work, only P branch lines corresponding to absorption from the ground state to the first vibrationally excited state were used. In addition, some of these lines were excluded, if they were too close to either neighboring second order CO transitions or lines resulting from ^{13}CO absorption or if the apparent peak intensity was less than 0.05 absorbance units. Tabulated listings of the positions of CO lines can be found from Rothman.[13] On the basis of these criteria, the temperature calculations performed in this work were based on P branch lines with m indexes between -5 and -35, excluding the lines with indexes of -10, -16, -17, -18, -19, -20, -24, -32, and -33. R branch lines have been excluded since they are not resolved from high temperature CO_2 lines. This will be of greater importance in the black liquor combustion environment.

Once the experimental or apparent peak heights of the lines to be used for temperature calculations were found, an iterative procedure was started. An initial estimate was made for the gas temperature and then this temperature was used to calculate the line width of the first absorption line using Equation 8 and the broadening coefficients and temperature exponents found in references 7, 10, 11, and 12. The data found in reference 10 are preferred if the initial estimate of temperature is in the range where these data apply, *i.e.*, above 500 K. Knowledge of the line half-width permitted the calculation of the resolution parameter, ρ, using Equation 6. Equation 4 was then used to calculate twenty values of A^a_{peak} given twenty different values of A^t_{peak}. These calculations were done by an adaptive Gaussian numerical integration routine. The range of A^t_{peak} values used yields A^a_{peak} values which cover the range of

possible apparent peak heights recorded by the instrument. This series of numerical integrations yielded the functional relationship between apparent and true peaks given a specific resolution parameter. A cubic spline interpolation routine was then used to get the specific true peak height which corresponds to the experimental peak. Once the true peak height was known for the first line, the calculations were repeated to obtain a half-width, a resolution parameter, and a true peak height for the next line. This procedure was continued until the true peak heights were determined for all the carbon monoxide absorption lines.

Once the true peak heights of all the lines were known, the temperature of the gas sample was calculated. This calculation was performed by making the plot described by Equation 2 and then calculating the best line to fit these data using a linear least squares routine. A first approximation of the gas temperature was then known, since the slope of this fitted line is equal to -1/T. The calculated temperature was then compared to the value of the estimated temperature used earlier to calculate the line widths. If the calculated temperature and the estimated temperature were within 0.1 K, the calculations were complete. If the two varied by more than 0.1 K, the estimated temperature was changed to the calculated value and the entire process was repeated, beginning with half-width calculations. Generally, 3-4 iterations were required to complete the calculations, which took approximately 10 minutes (total time) on a personal computer with a 16 MHz 80386 processor.

EXPERIMENTAL

Gas Cell

For these studies, the gas cell shown in Figure 1 was designed and constructed. It permits the acquisition of absorption spectra of gases at atmospheric pressure and at temperatures between 298 and 1273 K. The cell consists of a stainless steel tube with end caps; the inside diameter of the cell is 3 7/8" and the inside length is 3 3/4". Holes 5/8" in diameter are drilled through each end cap to allow the infrared beam to pass through the cell. The cell walls and end caps are constructed of 3/16" thick 304 stainless steel. Windows of 1" diameter yttrium oxide (Raytheon Corporation) or sapphire (General Ruby and Sapphire Co.) are contained in 2" diameter stainless steel window-holders and placed over the holes in each end cap. The windows are each wedged about 0.7^{o} to eliminate fringes in the absorption spectrum. Ceramic paper insulation (not shown in Figure 1) is used around the window and between the window-holder and gas cell to help seal the gas sample in the cell. Each window-holder is fastened to the end cap by stainless steel screws.

Inlet and outlet 0.157" I.D. stainless steel tubes were put into the cell to allow a continuous stream of gas to flow through the cell. The volumetric flow of individual CO and N_2 streams is controlled and monitored using rotometers. The two streams are mixed before entering the cell, and this mixture comprises the gas sample. This technique permits the gas sample composition to be accurately maintained. The inlet tube consists of a coil 72" long wound on the inside of the gas cell to preheat the gas to the cell temperature. Heat transfer calculations showed that the gas preheating is accomplished in the first few inches of the coil, which prevents significant cooling of the coil by the entering gas. A flow of gas continuously exits the cell through the outlet tube; this tube is open to the room so that the internal cell pressure is maintained at atmospheric pressure.

The gas cell is heated by placing it inside an electric tube furnace obtained from American Test Systems (ATS model 3110). The furnace has a maximum continuous temperature rating of 1273 K, a heated length of 4", an overall length of 5", an inside diameter of 4 1/2", and an overall diameter of 12". The temperature of the furnace is controlled by an LFE model 2010 time-proportioned temperature controller. Once inside the furnace, the ends of the gas cell are insulated with two discs made of B&W Kaowool HS-45 Board insulation placed over each of the end caps. The insulation was machined to an outside diameter of 8" and a thickness of 3". Holes through the center of each disc allow the infrared beam to pass through the cell. The insulation on the end caps was necessary to reduce energy loss through the ends of the cell.

Verification of Gas Cell Temperature

Despite the insulation, some heat losses can occur through the ends of the cell. Thus, a temperature gradient along the path of the infrared beam may be expected. Some concern also arose that the presence of the preheat coil could cause temperature gradients in the cell. In an effort to quantify these gradients, the temperature profile inside the cell was measured by placing the gas cell inside the tube furnace and putting ceramic paper windows in place of the normal sapphire or yttria windows. A small hole was placed in one of the ceramic paper windows to permit the penetration of a thermocouple into the cell. The thermocouple, supported by two ring stands, was put in place so that it could slide in and out of the furnace to any position within the gas cell. The thermocouple had an exposed junction and was obtained from the Omega Company (model XC1B-K-233).

A series of preliminary studies evaluated the magnitude of thermocouple errors resulting from radiative, conductive, and convective heat transfer to and from the thermocouple junction. No significant errors resulted from either radiation or convection. Radiative errors were checked by comparisons with a single layered shielded thermocouple. Convective errors were checked by varying the gas flow rate through the cell. While this method evaluated the influence of forced convection on temperature measurements, the importance of natural convection was not measured directly. However, because the temperature gradients within the cell are relatively small, and because the gas velocities resulting from natural convection would not be as high as the forced gas velocities, this error is assumed to be negligible. Thermocouple errors resulting from conduction were significant when the length of thermocouple inserted into the cell was less than one inch. This error tended to reduce the measured thermocouple temperature. The error was eliminated by recording two profiles, one originating from each end cap, and then excluding the first inch of temperature measurements from each profile in order to obtain the complete temperature profile.

Temperature profiles of the gas within the cell were obtained at seven different furnace set point temperatures: 373, 573, 773, 973, 1073, 1173, and 1273 K. Approximately ten temperatures were recorded for each profile along the cell centerline, and two profiles (one originating from each end of the cell) were recorded at each temperature. A typical temperature profile recorded at a furnace set point temperature of 1173 K is shown in Figure 2. The shape of this profile was similar for all temperatures (except for the 373 K profile which was flat) and agrees well with theoretical calculations performed to describe the temperature in the cell. The difference between the maximum and minimum temperatures along the profile was about 15 K when the furnace temperature was 1273 K, and this difference decreased as the furnace temperature decreased. An empirical equation was fit to each profile at each furnace set point temperature. This equation was integrated to obtain an average temperature which is used as a basis to compare with the temperatures calculated from absorption spectra.

Optics

The FT-IR spectrometer used for this study was a Laser Precision Analytical model RFX-75. The instrument is capable of a maximum nominal resolution of 0.125 cm^{-1}, although in this work all the spectra were recorded at 0.25 cm^{-1} in order to reduce the data acquisition time. The resolution of the instrument at this nominal resolution setting was determined by first measuring the full width at half height (FWHH) of triangularly apodized, low pressure CO absorption lines. These spectra were recorded using a standard 10 cm gas cell with 25 x 4 mm CaF_2 windows (Janos Technology Inc.). The FWHH of these lines was found to be 0.22 cm^{-1}. It is assumed that their width is primarily due to instrument broadening, since the pressure within the cell (< 10 torr) was maintained well below the regime where collisional broadening becomes important. The resolution of the instrument is defined as the distance between the peak maximum and the point where the LS reaches the baseline for the first time. This distance was determined by plotting the sinc squared function, $\sin^2(x \cdot \pi \cdot C)/(x \cdot \pi \cdot C)^2$, and adjusting C until the FWHH of this calculated LS was 0.22 cm^{-1}. The distance between the peak maximum and the point where this calculated curve first touched the baseline was found to be 0.25 cm^{-1}, which is then defined as the resolution of the instrument.

Because of the furnace size and the high temperatures, no conventional sample compartment could be used to contain the gas cell. Instead, the beam is directed from the interferometer to the cell by a series of mirrors, as shown in Figure 3. After exiting the interferometer as a 1" diameter collimated beam, the infrared source is gathered and focused by an 8" focal length parabolic mirror. The beam is focused through an 800μm aperture and is received by a second 8" focal length mirror (located 16" away from the first) which sends the beam collimated to a third 8" focal length mirror. This third mirror directs the beam through the gas cell. The beam is then picked up on the other side of the gas cell by a fourth 8" mirror which sends the beam collimated to a flat mirror which directs the beam into a wideband 0.25 mm mercury-cadmium-telluride (MCT) detector. Inside the detector, the collimated beam strikes one final mirror which focuses it onto the detector chip. This optical configuration keeps the furnace sufficiently far from the interferometer while minimizing the number of reflections. The mirrors were obtained from Laser Precision Analytical and were part of their external optical component system called Optibus. This system of mirrors offers a convenient means of transferring the infrared beam, since the pieces are prealigned and are simply clamped together. It further provides a way to control the environment between the interferometer and the gas cell.

The aperture located between the first and second mirrors is used to reduce the effect of stray emission on the absorption spectra. Without the aperture, emission from the gas sample can go back through the Optibus components to the interferometer, become modulated, and then go back through the mirrors, through the cell and to the detector. This emission radiation has been observed in absorption spectra recorded in the absence of the aperture. Placement of the aperture between the first and second mirrors eliminated this source of error.

Data Collection

CO absorption spectra were collected at a nominal instrument resolution of 0.25 cm^{-1}, and either 250 or 500 scans were averaged to obtain a single well-resolved spectrum. The data collection times were 7 and 14 minutes, respectively. Triangular apodization and 15-X zero filling were used to obtain the final spectrum. Triangular apodization was applied, since the convolution of the line shape resulting from this apodization function and the Lorentzian line profile is easily numerically integrated. A high degree of zero filling was used to improve the accuracy of selecting the peak maximum resulting from the experimental spectrum. The gas samples consisted of 1, 3, 5, or 10% by volume CO in nitrogen. A gas flow at a volumetric flow rate of 1.0 L/min was continuously passed through the cell. Before they were mixed, the CO and nitrogen flow rates were separately metered using Brooks rotometers (model 1355-V).

RESULTS AND DISCUSSION

High Temperature CO Absorption Spectra

Absorption spectra of CO/N_2 gas mixtures were recorded at furnace set-point temperatures of 297, 373, 573, 773, 973, 1073, 1173, and 1273 K. The gas temperatures corresponding to furnace set-points were 297, 361, 547, 746, 948, 1048, 1149, and 1251 K, respectively, as measured by a thermocouple. Six spectra were recorded at each temperature except at 297 K and 1273 K where nine and twelve spectra were recorded, respectively. Figures 4-6 show typical absorption spectra of the P branch of CO at furnace set-point temperatures of 573, 1073, and 1273 K; the CO concentration in each of these three samples was 5%. These three spectra are representative of the quality of all the absorption spectra recorded using the high temperature gas cell. In general, the spectra had an excellent signal-to-noise ratio; the peaks were very well resolved, and there was no evidence of emission peaks. This suggests that the placement of an aperture with a diameter of 0.8-1.6 mm was effective in stopping modulated emission from the hot gases from reaching the detector.

The spectra shown in Figures 4-6 illustrate both the changes in absorption behavior which occur at increasing temperatures and the effects of some experimental factors. First, among the experimental effects, the signal-to-noise ratio decreased as the temperature increased. This is a consequence of the

diminished transmission of infrared radiation through the yttrium oxide windows at the higher temperatures. This same effect has been observed with sapphire windows. The changing transmission properties of the windows requires that background spectra be recorded at the same temperature as the sample spectra. For these spectra, a new background spectrum was collected before each sample spectrum.

The spectra shown in Figures 4-6 also illustrate the changing absorption behavior of CO at increasing temperatures. First, as the temperature of the gas increases, the intensity of the second order transitions increases; these are transitions from the first vibrationally excited state to the second excited state. These lines appear as a P branch band with a shape that is similar to the first order band, but with frequencies shifted to lower wavenumbers. Second, as the temperature increases, the number of molecules populating the energy levels corresponding to higher |m| values increases. This results in both a lowering of the intensity of the lines with low |m| values and a simultaneous increase in the intensity of lines of higher |m| values. In the spectra this appears as an overall reduction in the peak intensities combined with an increase in the number of lines observed on the outer wing of the P branch band. It is this temperature-dependent shift in line intensities as a function of |m| that yields the information for obtaining temperatures from Equation 1.

Figures 4-6 also illustrate the need for selectivity in choosing absorption lines for temperature calculations. As the second order transitions increase in intensity, lines which are not fully resolved from the first order lines will influence the peak heights of the first order peaks. Note, for example, the m = -18 line (2068.847 cm^{-1}) in Figures 4 and 5. At 746 K this peak is only slightly above the contour of neighboring lines while at 1048 K this peak is clearly distorted by the second order m = -12 peak (2068.803 cm^{-1}). Inclusion of this peak in the temperature calculations will result in incorrect temperature determinations. In general, first order CO peaks which were within 0.5 cm^{-1} of either a ^{13}CO or second order ^{12}CO peak were excluded from temperature calculations. While this required separation is greater than the 0.25 cm^{-1} dictated by the resolution of the instrument, this restriction only resulted in the exclusion of four additional lines with m values of -16, -17, -20, and -33. These lines were 0.287, 0.261, 0.417, and 0.343 cm^{-1}, respectively, from the nearest interfering line.

Temperature Calculations

Gas temperatures were calculated from the fifty-seven spectra using the program described in the Temperature Calculation Methodology section. The results are presented in Table I. Included in this table is a comparison of gas temperatures determined from spectra to gas temperatures measured by a thermocouple. The difference between the two is reported as both an average ΔT and an average percent difference. This table also includes the statistical information (high, low, mean, and standard deviation) regarding the replicates at each temperature.

The data in Table I have not been segregated at each temperature, depending upon the CO concentration. There was no significant difference in the calculated temperatures for the different concentrations. Although this was expected, since Equation 1 contains no concentration dependent terms, it is important to note that this is verified by the data, since gas concentrations will not always be known in the combustion environment.

Good agreement between thermocouple and spectroscopic temperatures was observed. The average percent differences between the two vary between 0.5 and 3.2%. The variation among spectra at a given temperature was acceptably small. At temperatures below 1149 K, the standard deviation of the six or nine spectra recorded at each temperature did not exceed 4 K. At higher temperatures, 1149 and 1251 K, the standard deviation increased to 9.5 and 20.3 K, respectively. The increase of standard deviations at higher temperatures is probably a result of the reduced signal-to-noise ratio in these spectra and the corresponding increased random variation of experimental peak heights. This variation is evident in the 1251 K spectrum shown in Figure 6.

In addition to sample variation, error is associated with the measurement of the gas temperatures by thermocouples. First, the K type thermocouples used for the temperature profiling have an uncertainty of ± 0.75% (as reported by the thermocouple manufacturer). Variations in packing the insulation around the gas cell can lead to variation in the energy loss, which can thus also change the temperature profile. The combined error associated with the thermocouple uncertainty and insulation was evaluated by determining the temperature profile with a thermocouple at a furnace set-point temperature of 1273 K on five different days. The gas temperatures from these profiles were 1254, 1253, 1251, 1245, and 1249 K, which yielded an average value of 1250 K with a standard deviation of 13 K. This variation, combined with the variation between samples, can account for the error at the higher temperatures of 1149 and 1251 K, but perhaps does not account for the variation at lower temperatures.

Presented in Figures 7 and 8 are representative samples of $\ln(A^{\dagger}_{peak}(m) \cdot \gamma(m)/(|m| \cdot F(m) \cdot \nu(m)))$ vs. $E(m)/k$ plots at each furnace set-point temperature. Figure 7 contains plots for spectra recorded at furnace set-point temperatures of 296, 373, 573, and 773 K, and Figure 8 contains plots for spectra recorded at temperatures of 973, 1073, 1173, and 1273 K. An arbitrary constant has been added to the y-coordinates of several of the data sets making up the lines in these two figures in order to separate the lines for visual clarity. In Figure 7 the constants -1, 2.5, and 4.5 have been added to the y-coordinates in the 297, 573, and 773 K plots, respectively. In Figure 8 the constants -1.5, 1.5, and 2.5 have been added to the y-coordinates in the 973, 1173, and 1273 K plots, respectively. The differences between the slopes, which reflect the different temperatures, are made more obvious by the separation.

At all temperatures these plots are quite linear. The spectra recorded at the higher temperatures resulted in plots which deviate slightly from this high degree of linearity. This appears to be a result of the reduced signal-to-noise ratio present in these spectra and the corresponding increases in random variations of the peak heights. It should be noted that this linear behavior was obtained only after correcting for photometric errors and line broadening. Prior to making these corrections, the plots were linear over a limited range of E(m)/K but exhibited significant nonlinearities at the extreme lower values of E(m)/K. The calculation of slopes from these nonlinear plots yielded calculated temperatures which were significantly in error.

Variation Between Thermocouple and Calculated Results

Variations in thermocouple measurements and random sample variations alone cannot account for the differences calculated at furnace temperatures of 361, 547, 746, 948, and 1048 K. Nor can such errors account for the tendency of all the calculated spectral temperatures to be lower than the gas temperatures measured by the thermocouple. In all cases, the average calculated temperature was below the thermocouple temperature. Figure 9 is a plot of the average calculated temperatures compared to the temperatures recorded using the thermocouple. The data appeared to be skewed to lower calculated temperatures by the influence of some additional factor.

It has been suggested that the use of a linear least squares fit of the data can lead to inaccuracies in temperature calculations since the standard deviation of the y term in the temperature plots, $\ln(A^{\dagger}_{peak}(m) \cdot \gamma(m)/(|m| \cdot F(m) \cdot \nu(m)))$, varies with $E(m)/k$.[7] The linear least squares model assumes that all the variances for the y components are equal. Generally, the y terms are weighted to compensate for this deviation to meet the model requirements. In an effort to determine the importance of weighting, the y-components of some plots were weighted by the inverse of the variance of y. The temperatures were then recalculated for several of the spectra. The weighting resulted in only minor changes in the calculated temperatures, changes that were not always in the direction closer to the temperatures measured by a thermocouple. Therefore, it appears unlikely that the use of an unweighted least squares is responsible for the systematic lowering of the calculated temperatures.

It was also possible that modulated emission from the gas samples, if it reached the detector, might be biasing the data. The aperture placed between the gas cell and the interferometer was effective in eliminating most of the emission radiation which becomes modulated. The importance of the remaining

emission which reached the detector was evaluated by performing calculations with theoretical spectra. Two spectra were calculated, one for CO absorption and the other for emission, each at 1273 K. The emission spectrum peak heights were normalized to reduce their heights to 25% the intensity of the absorption peaks. The emission peaks (negative peaks) were then added to the absorption spectrum, and the temperature of the resulting spectrum was calculated. The calculated temperature was higher than 1273 K, while the plot of $\ln(A^t_{peak}(m) \cdot \gamma(m)/(|m| \cdot F(m) \cdot \nu(m)))$ vs. $E(m)/k$ remained linear. This would suggest that the deviations observed in the calculated temperatures, which are in the opposite direction, are not a result of emission. However, it is likely that the 1149 and 1251 K spectra are slightly affected by modulated emission, which has resulted in raising the calculated temperatures closer to the measured gas temperatures as shown in Figure 9. The emission may be reducing the percent differences between the calculated and measured gas temperatures at these two furnace set points. The higher temperature spectra would be more affected by emission, since it is at these temperatures that emission from the gas sample is greatest.

The significance of emission can be further explored by considering the results of changing the aperture diameter used to block the modulated emission from reaching the detector. As the diameter of the aperture was increased, the calculated temperatures also increased. With no aperture in place, the calculated temperatures were 50-100 K above the measured temperatures at the higher furnace set point temperatures. Therefore, it is unlikely that emission from the gas sample is causing the lowering of the calculated temperatures. However, it is very likely that it is responsible for reducing the difference between calculated and measured gas temperatures at the higher furnace set-point temperatures.

Of the eight temperatures examined, the best results were obtained at room temperature. The high degree of accuracy obtained at this temperature suggests that the calculation methodology is correct. This is also the only temperature at which line widths have been experimentally measured. At all other temperatures, a model is used to estimate the widths of the lines. It is possible that inaccuracies in the estimates of the line widths are responsible for the deviations between calculated and measured gas temperatures. The temperature calculation program is very sensitive to changes in ρ, the ratio of the instrument resolution to the line width. The line width data of Hartmann *et al.*[10] has an accuracy of $\pm$ 10%. Altering only a few of the line widths by this amount has been shown to result in significant changes in the calculated temperatures ($\pm$ 20 K). Clearly, changes of line widths of this magnitude could account for the discrepancies between calculated and measured gas temperatures.

CONCLUSIONS

Temperature calculations have been successfully derived from CO absorption spectra at temperatures up to 1273 K. These calculations had accuracies of 3.2% or better as compared to thermocouple measurements (accuracy of $\pm$ 0.75%) and were found to be independent of CO concentration. The accuracy of these calculations met the expectations of the technique in this high temperature environment and will be sufficiently reliable to be used in combustion research. The success of these calculations can be attributed to two factors; first, the high degree of linearity of the lines in Figures 7 and 8, and second, control of the emission from the hot gases. The high degree of linearity of the lines in Figures 7 and 8 has resulted from correctly accounting for the photometric error. Before these corrections were made, the plots of $\ln(A^t_{peak}(m) \cdot \gamma(m)/(|m| \cdot F(m) \cdot \nu(m)))$ vs. $E(m)/k$ were significantly curved. A fitted straight line to these plots resulted in poor regression coefficients and calculated temperatures in error by 10-20%. Reliable half-width broadening data from Hartmann *et al.*[10] have also been key components toward the results shown in Figures 7 and 8. Although we attribute some of the error of these calculations to the inaccuracies of this model ($\pm$ 10%), in general, the model has done an adequate job of predicting CO line broadening by nitrogen. We have found this model to be the most comprehensive and accurate source of high temperature CO line broadening information.

The second key component for accurate temperature calculations has been the control of emission from the hot gases. The use of an aperture in the optical path has eliminated the presence of emission peaks

in the absorption spectra and has significantly reduced calculation errors resulting from the use of absorption spectra with absorption peaks convoluted with emission lines.

These calculations represent only the first phase of work in a project whose ultimate objective is to use FT-IR absorption spectroscopy for the *in situ* determination of gas temperatures and concentrations above a burning black liquor char bed. In the next phase, the concentration of the CO and CO_2 will be determined from CO and CO_2 absorption spectra recorded from the high temperature gas cell.

ACKNOWLEDGMENTS

The authors gratefully acknowledge the financial support obtained from the U.S. Department of Energy under grant DE-ACO2-83CE40637 and also that obtained from the Institute of Paper Science and Technology and its member companies. We also acknowledge the generous technical support offered by the personnel of Laser Precision Analytical. We also are indebted to Raytheon Corporation for their donation of the yttria windows. Finally, the authors wish to thank Professor James A. de Haseth of the University of Georgia, Athens, for several helpful suggestions.

Portions of this work were used by Patrick J. Medvecz as partial fulfillment of the requirements for the Ph.D. degree at the Institute of Paper Science and Technology.

LITERATURE CITED

1. D. K. Ottesen and D. A. Stephenson, Combustion and Flame **46**, 95 (1982).

2. L. R. Thorne and D. K. Ottesen, Proc. - Electrochem. Soc. **83-7**, 425 (1983).

3. D. K. Ottesen and L. R. Thorne, Proc. - Int. Conf. Coal Sci, 351 (1985).

4. P. R. Solomon, D. G. Hamblen, R. M. Carangelo, and J. L. Krause, "Coal Thermal Decomposition in an Entrained Flow Reactor; Experiment and Theory," 19th Symposium (International) on Combustion, 1139, Pittsburgh, PA (1982).

5. T. A. Cleland and D. W. Hess, J. Appl. Phys **64**, 1068 (1988).

6. R. J. Anderson and P. R. Griffiths, J. Quant. Spectrosc. Radiat. Transfer **17**, 393 (1977).

7. L. A. Gross, P. R. Griffiths, and J. N.-P. Sun, "Temperature Measurement by Infrared Spectrometry," in *Infrared Methods For Gaseous Measurements*, J. Wormhoudt, Ed. (Marcel Dekker, Inc., New York, New York, 1985), Chap. 3.

8. R. J. Anderson and P. R. Griffiths, Anal. Chem. **47**, 2339 (1975).

9. P. R. Griffiths and J. A. de Haseth, *Fourier Transform Infrared Spectrometry* (John Wiley & Sons, New York, 1986), p. 18.

10. J. M. Hartmann, L. Rosenmann, M. Y. Perrin, and J. Taine, Appl. Opt. **27**, 3063 (1988).

11. P. L. Varghese and R. K. Hanson, J. Quant. Spectrosc. Radiat. Transfer **24**, 479 (1980).

12. T. Nakazawa and M. Tanaka, J. Quant. Spectrosc. Radiat. Transfer **28**, 409 (1982).

13. L. S. Rothman, Appl. Opt. **20**, 791 (1980).

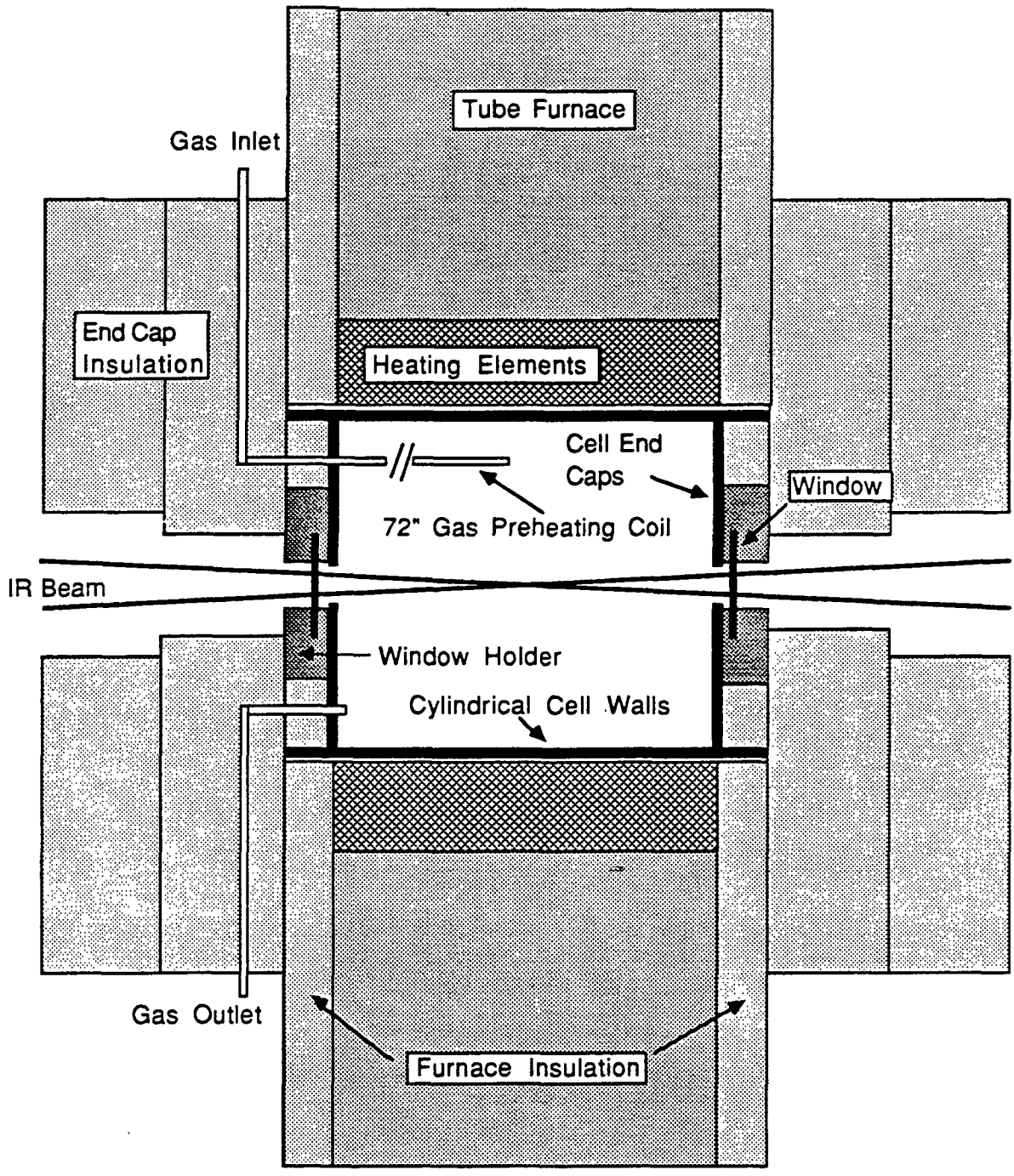

Fig. 1. Schematic diagram of high temperature gas cell. Also shown are the tube furnace, heating elements, end cap insulation, and the path of the infrared beam.

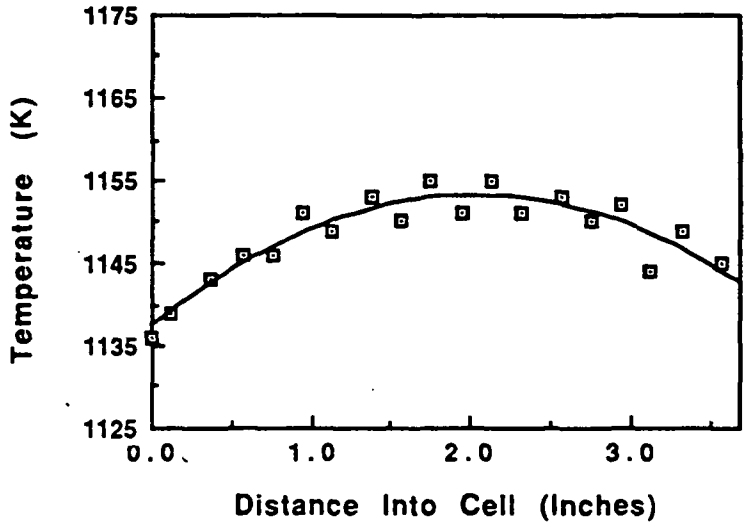

Fig. 2. Gas temperature profile within the gas cell at a furnace set-point temperature of 1173 K.

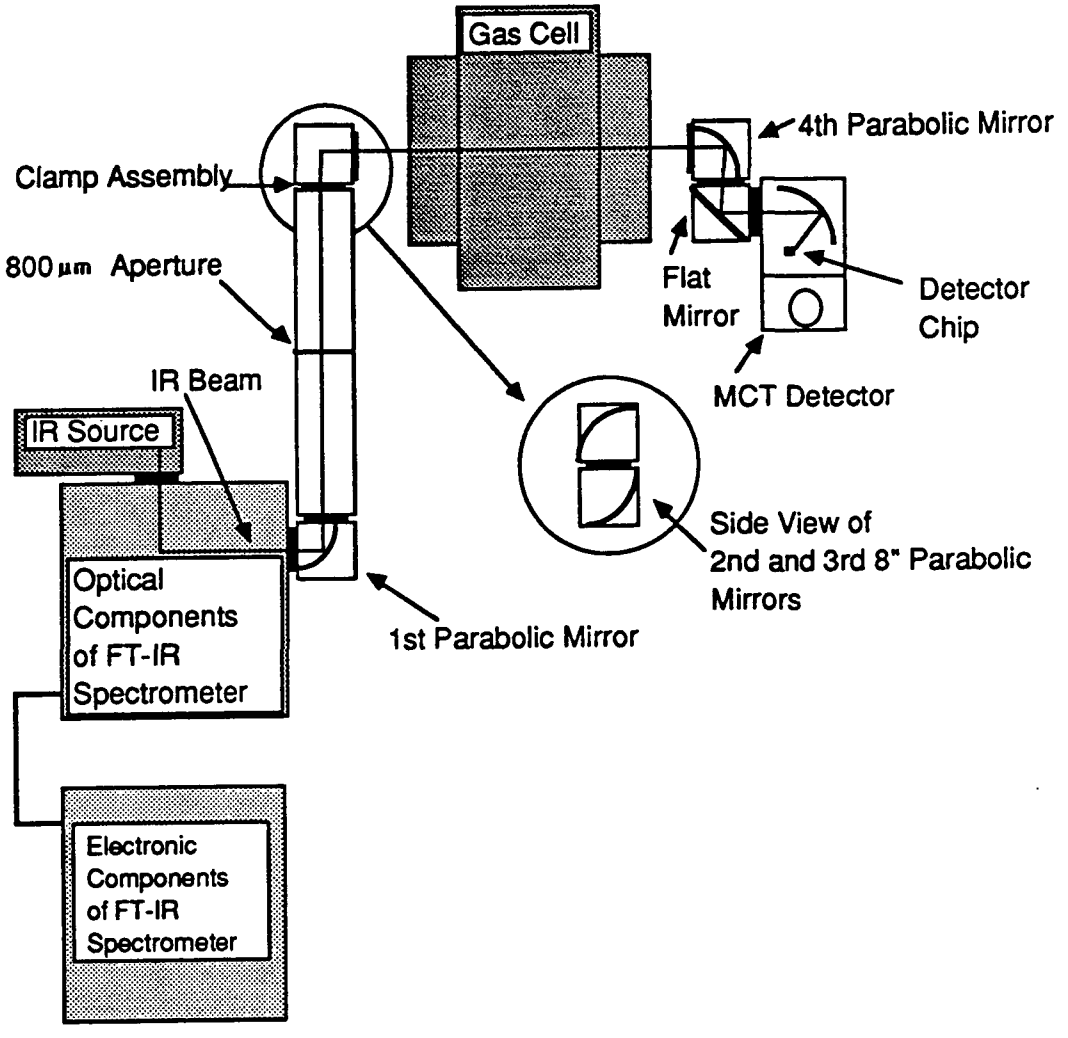

Fig. 3. Overhead diagram of optical configuration including the FT-IR, Optibus components, high temperature gas cell, and MCT detector.

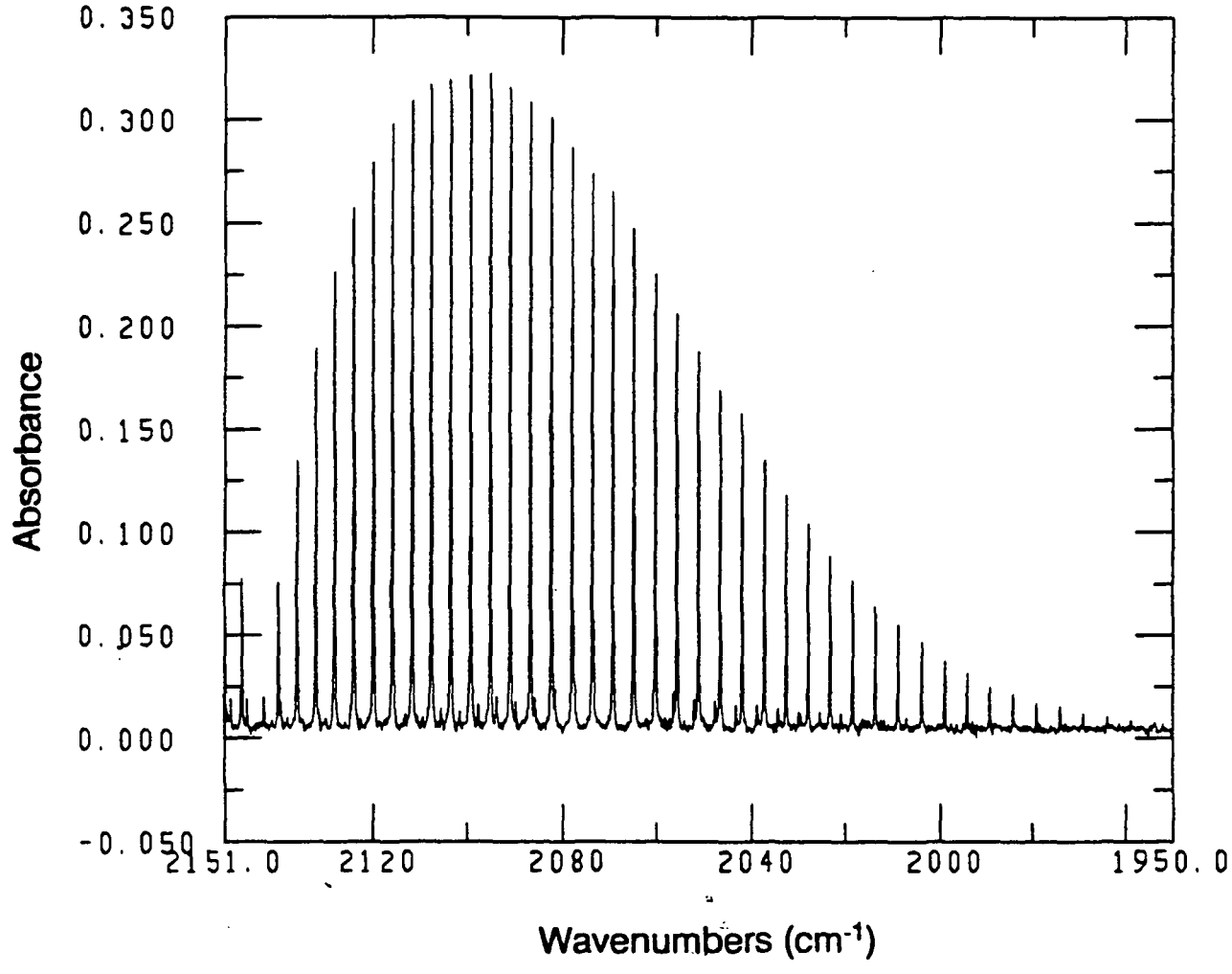

Fig. 4 CO absorption spectrum at 746 K.

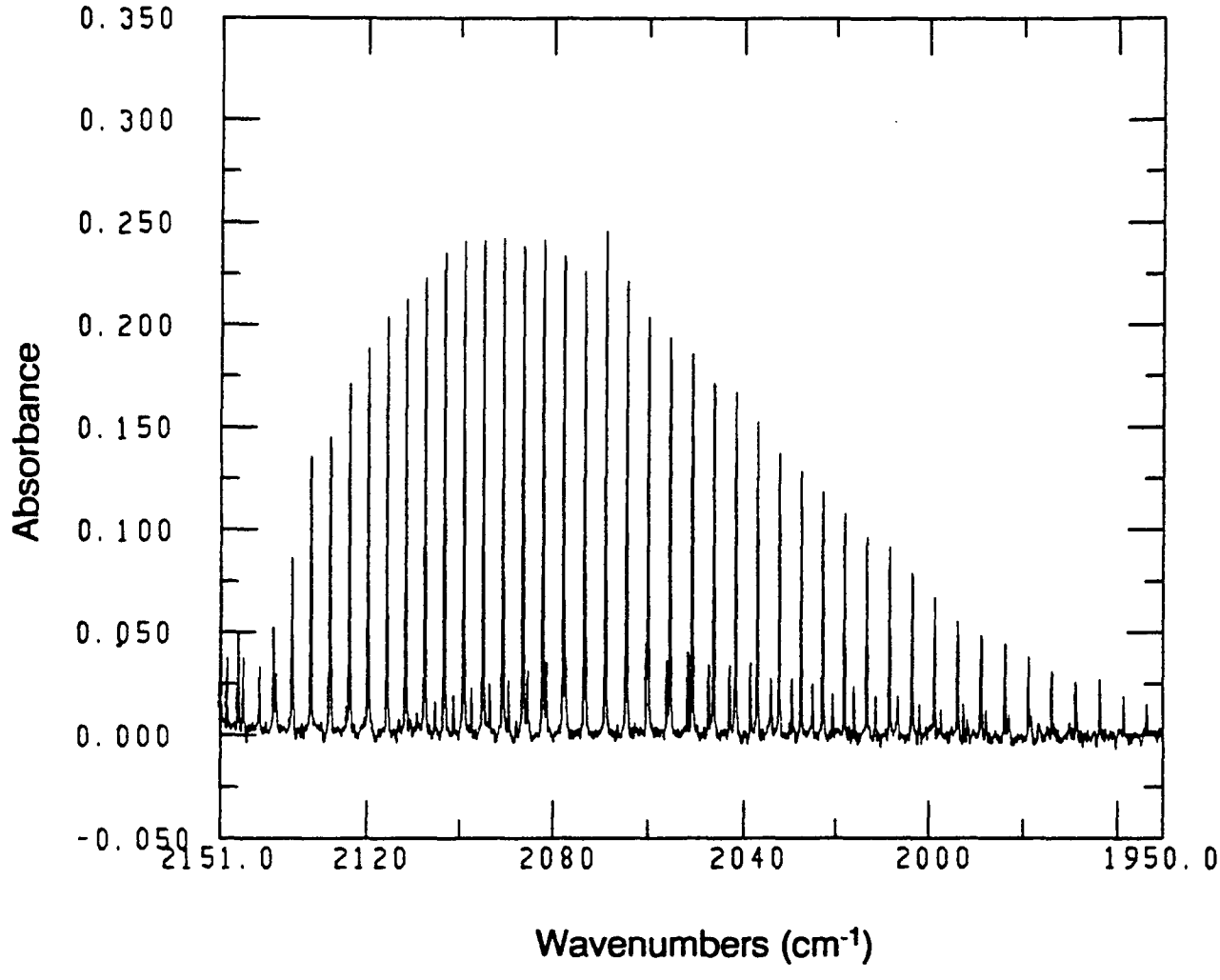

Fig. 5 CO absorption spectrum at 1048 K.

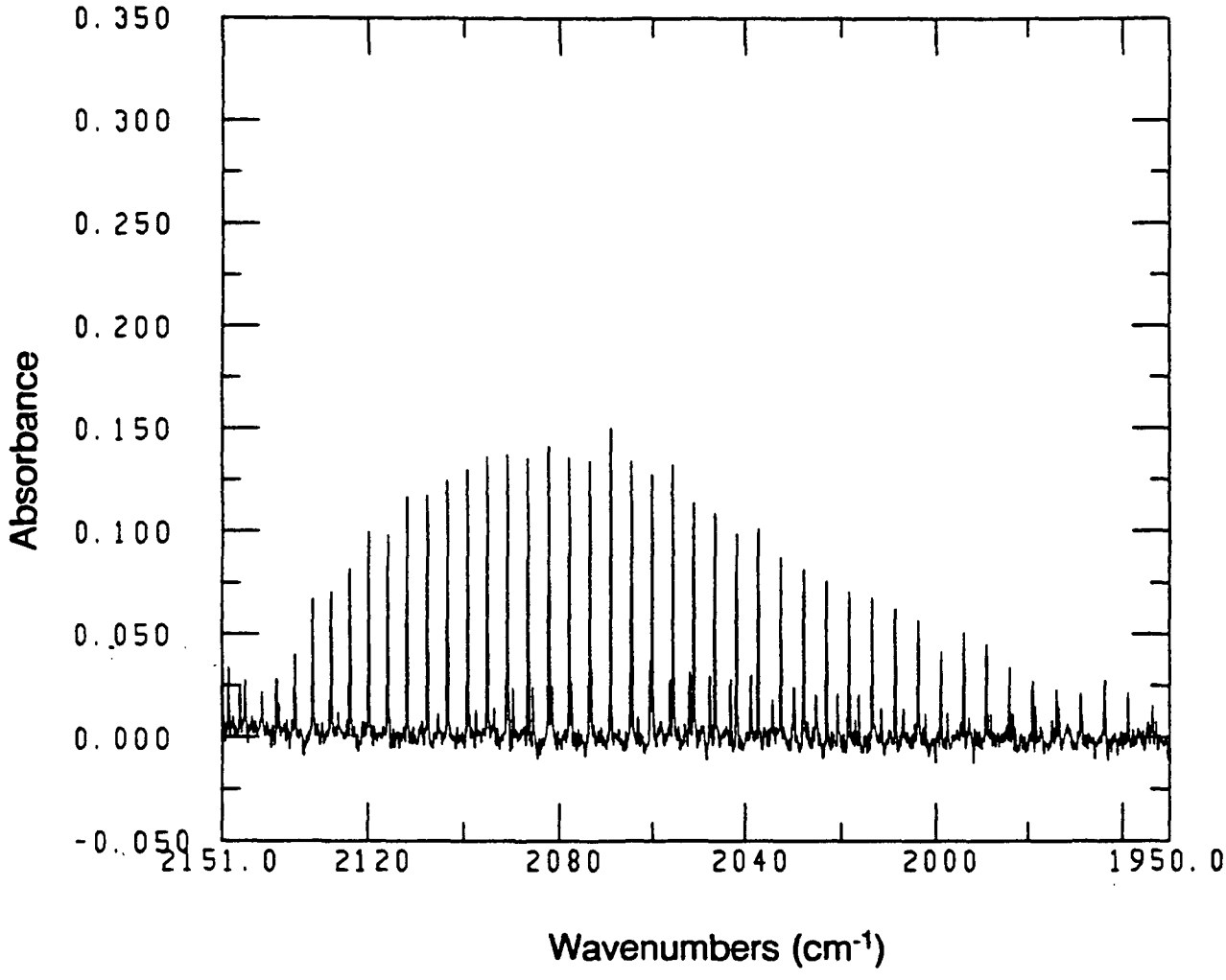

Fig. 6 CO absorption spectrum at 1251 K.

TABLE I. Results of Temperature Calculations from CO Absorption Spectra.

Furnace Set Point	Number of Spectra	Average Thermocouple Temp.	Average Calc. Temp.	Average Absolute Difference	Percentage Absolute Difference	Low	High	σ, (K)
297 K	9	297 K	296 K	1.6 K	0.5%	294 K	298 K	1.5
373 K	6	361 K	352 K	9 K	2.6%	349 K	353 K	1.4
573 K	6	547 K	533 K	14 K	2.6%	530 K	537 K	2.9
773 K	6	746 K	731 K	15 K	2.0%	727 K	735 K	3.7
973 K	6	948 K	917 K	31 K	3.2%	912 K	921 K	3.6
1073 K	6	1048 K	1021 K	27 K	2.5%	1020 K	1024 K	1.7
1173 K	6	1149 K	1132 K	17 K	1.5%	1117 K	1146 K	9.5
1273 K	12	1251 K	1234 K	21 K	1.7%	1202 K	1267 K	20.3

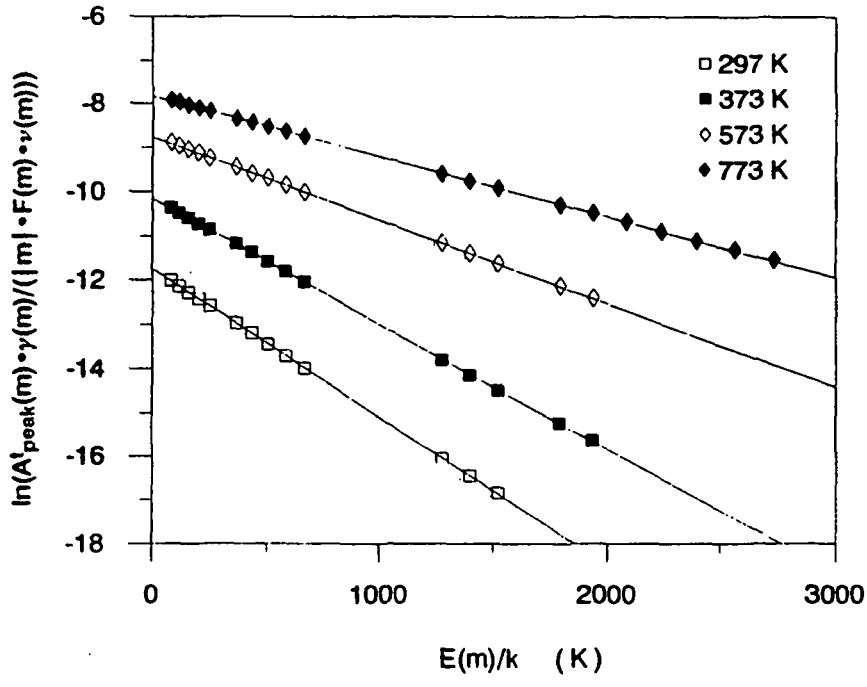

Fig. 7 Plot of $\ln(A^{t}_{peak}(m)\cdot\gamma(m)/(|m|\cdot F(m)\cdot\nu(m)))$ vs. E(m)/k for representative spectra recorded at furnace set-point temperatures of 297, 373, 573, and 773 K.

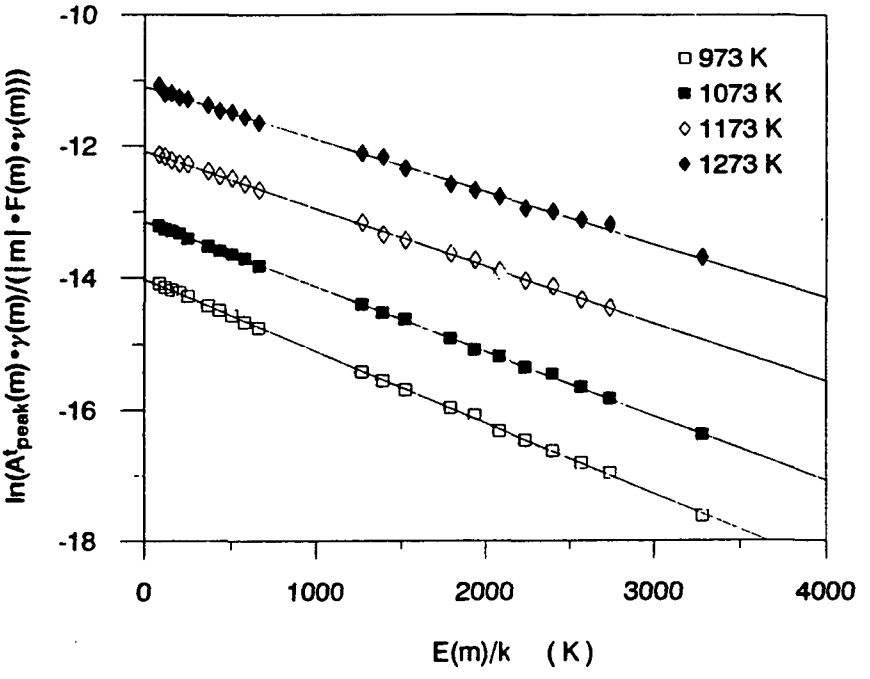

Fig. 8 Plot of $\ln(A^{t}_{peak}(m)\cdot\gamma(m)/(|m|\cdot F(m)\cdot\nu(m)))$ vs. E(m)/k for representative spectra recorded at furnace set-point temperatures of 973, 1073, 1173, and 1273 K.

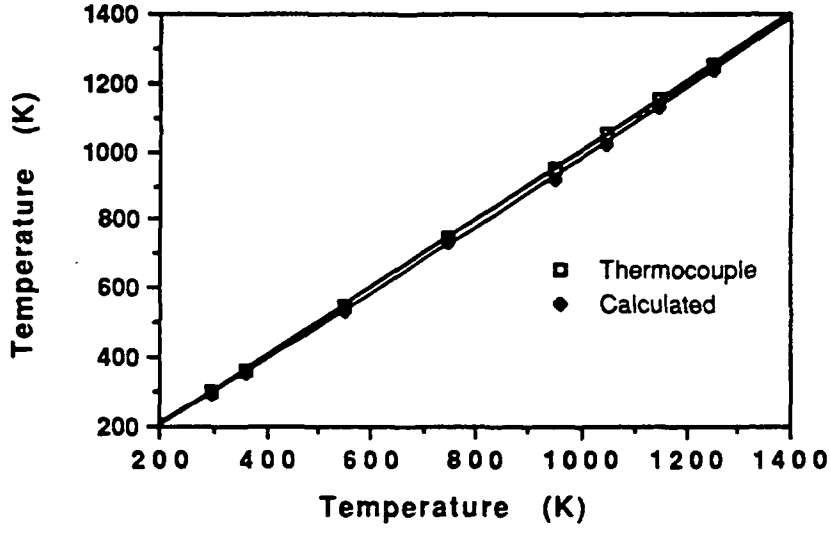

Fig. 9 Plot of gas temperatures measured by a thermocouple compared to gas temperatures calculated from CO absorption spectra.